ORIGINAL PAPER

Detecting short-term stress and recovery events in a vineyard using tower-based remote sensing of photochemical reflectance index (PRI)

Christopher Y. S. Wong[1] · Nicolas E. Bambach[2] · Maria Mar Alsina[3] · Andrew J. McElrone[4,5] · Taylor Jones[6] · Thomas N. Buckley[1] · William P. Kustas[7] · Troy S. Magney[1]

Abstract

Frequent drought and high temperature conditions in California vineyards necessitate plant stress detection to support irrigation management strategies and decision making. Remote sensing provides a powerful tool to continuously monitor vegetation function across spatial and temporal scales. In this study, we utilized a tower-based optical-remote sensing system to continuously monitor four vineyard subplots in California's Central Valley. We compared the performance of the greenness-based normalized difference vegetation index (NDVI) and the physiology-based photochemical reflectance index (PRI) to track variations of eddy covariance estimated gross primary productivity (GPP) during four stress events between July and September 2020. Our results demonstrate that NDVI was invariant during stress events. In contrast, PRI was effective at tracking the short-term stress-induced declines and recovery of GPP associated with soil water depletion and increased air temperature, as well as reductions in GPP from decreased PAR caused by smokey conditions from nearby fires. Canopy-scale remote sensing can provide continuous real-time data, and physiology-based vegetation indices such as PRI can be used to monitor variation of photosynthetic activity during stress events to aid in management decisions.

Introduction

Water management is critical in California vineyards as water deficits, high temperatures and high vapor pressure deficits (VPD) occur frequently and are often a key limiting factor in productivity and yield (Draper et al. 2003; Tanaka et al. 2006). Climate change will further exacerbate drought and high temperature conditions leading to increased frequencies and severity of major stress events (Strzepek et al. 2010; Ficklin and Novick 2017). Therefore, it is important to employ appropriate irrigation strategies to maintain productivity and yield (Matthews and Anderson 1989; Reynolds and Naylor 1994; Jones and Davis 2000) and also to improve grape quality (Chaves et al. 2010). Real-time assessment of plant stress will be essential for improving irrigation management.

Drought stress results in physiological responses influencing grapevine function (Gambetta et al. 2020), including reduced stomatal conductance (Flexas et al. 1998; Buckley 2019), osmotic adjustment (Patakas and Nortsakis 1999; Blum 2017), altered pigment composition (Jaleel et al. 2009), and chloroplast movement (Kasahara et al. 2002), all of which can ultimately influence photosynthetic activity (Reddy et al. 2004; Chaves et al. 2009). To address this, different approaches have been developed for real-time detection of drought stress. One standard indicator of water stress is leaf or stem water potential measured with pressure chambers (Girona et al. 2006). This approach, however, is labor intensive, error prone from subjectivity, and destructive, limiting its practicality over large areas with high temporal frequency. Thus, there is significant interest in employing

✉ Troy S. Magney
tmagney@ucdavis.edu

1 Department of Plant Sciences, University of California, Davis, CA 95616, USA

2 Department of Land, Air, and Water Resources, University of California, Davis, CA 95616, USA

3 Department of Winegrowing Research, E & J Gallo Winery, Modesto, CA 95354, USA

4 Crops Pathology and Genetics Research Unit, USDA-ARS, Davis, CA 95616, USA

5 Department of Viticulture and Enology, University of California, Davis, CA 95616, USA

6 Department of Earth and Environment, Boston University, Boston, MA 02215, USA

7 Hydrology and Remote Sensing Lab, USDA-ARS, Beltsville, MD 20705-2350, USA

remotely sensed products for monitoring plant water stress at high spatial and temporal resolutions (Ihuoma and Madramootoo 2017).

Two main remote sensing approaches have been used to track physiological changes in vineyards: thermal infrared- and optical-based remote sensing. Thermal infrared-based remote sensing measures canopy surface temperature, which is strongly influenced by evaporative cooling and hence stomatal conductance (Khanal et al. 2017) and can be used to serve as an indicator of water stress (González-Dugo et al. 2006). The crop water stress index (CWSI), which is based on differences between air and canopy temperatures (Jackson et al. 1981), has been used to quantify plant water stress (Jackson et al. 1988; Prueger et al. 2019). However, data are often taken during a small time window (close to solar noon and clear skies) and require crop-specific baseline calibrations that may further vary across weather conditions and time (Alves and Pereira 2000). While thermal-based approaches have been shown to be a useful tool for estimating evapotranspiration (ET) and stress, the capability of these methods to determine plant stress using satellite data can be limited by latency issues and the pixel resolution of thermal infrared sensors (Knipper et al. 2019b; Bellvert et al. 2020). Alternatively, optical-based remote sensing has emerged as a viable option to infer information about canopy structure and function (Ustin et al. 2004; Blackburn 2007). The normalized difference vegetation index (NDVI) is commonly used to assess canopy structure and light harvesting (Myneni and Williams 1994; Carlson and Ripley 1997). NDVI has shown promise for detecting vegetation response to drought stress (Peters et al. 2002; Ji and Peters 2003; Gu et al. 2008). However, NDVI largely reflects changes in canopy structure due to leaf movement, wilting and chlorophyll degradation (Gitelson et al. 2014). Therefore, physiology-based vegetation indices may better serve to capture dynamic changes in leaf pigment composition that are associated with photosynthetic activity and stress (Ustin et al. 2004; Blackburn 2007).

The photochemical reflectance index (PRI) is sensitive to changes in the xanthophyll cycle and often used as a proxy of photosynthetic efficiency (Gamon et al. 1992, 1997; Peñuelas et al. 1995). The xanthophyll cycle involves conversion of the carotenoid pigment violaxanthin to antheraxanthin and zeaxanthin to dissipate excess absorbed energy when photosynthesis becomes saturated or limited under stress conditions; this conversion reverses upon recovery, typically at daily timescales (Demmig-Adams and Adams 1996). At seasonal timescales, PRI is sensitive to the ratio of carotenoid to chlorophyll pigment pools but remains a good indicator of seasonal photosynthetic activity (Garrity et al. 2011; Wong and Gamon 2015). Since PRI is sensitive to both short- and long-term physiological variation of carotenoid pigments (Gamon and Berry 2012), it may provide a robust indicator of seasonality, short-term stress, and prolonged stress events. However, due to this sensitivity across temporal scales, PRI may require disentangling to separate short-term vs long-term signal contributions to optimize PRI performance (Hmimina et al. 2015). In this context, recent studies have highlighted the short-term sensitivity of PRI for reflecting drought stress in agricultural cropping systems like tomatoes, nut and fruit tree orchards, quinoa, wheat, and vineyards (Thenot et al. 2002; Zarco-Tejada et al. 2005, 2013; Suárez et al. 2008; Sarlikioti et al. 2010; Magney et al. 2016). Therefore, for grapevines, we hypothesize that by disentangling the long- and short-term PRI signal, PRI will reflect both seasonal variation and dynamic variation in photosynthetic activity due to stress events as well as the subsequent recovery.

In this study, we deployed a scanning tower-based optical spectrometer system to continuously monitor four vineyard subplots in California's Central Valley from July 19 to September 23, 2020. We identified the occurrence of four stress events based on a short-term decline and recovery represented by gross primary productivity (GPP) variation estimated by eddy covariance. Assuming that stress events influence physiological mechanisms regulating photosynthetic activity and thus GPP, vegetation indices derived from optical-based remote sensing may perform as proxies of GPP variation during short-term stresses. Our objectives were to apply a simple detrending analysis to disentangle long- and short-term variation of NDVI and PRI to (1) evaluate the performance of NDVI and PRI for reflecting short-term stress events; and (2) and evaluate potential hysteresis effects between GPP and NDVI, and PRI during stress response and recovery.

Methods

Vineyard

This study is part of the USDA-ARS Grape Remote Sensing Atmospheric Profile and Evapotranspiration eXperiment (GRAPEX) (Kustas et al. 2018) conducted at a commercial vineyard block in California's Central Valley. The vineyard block was planted with merlot (*Vitis vinifera* L.) in 2010 and trained on a split trellis. It contains a variable rate drip irrigation (VRDI) system that allows delivery of irrigation amounts to vary at 30 m resolution. The vineyard block (RIP720) was divided into four subplots (with subplots referred to as RIP1–RIP4) each approximately four hectares in size representing northwest (RIP1), northeast (RIP2), southwest (RIP3), and southeast (RIP4) quadrants. Soil type is loam/sandy loam. The vineyard subplots have maximum canopy heights ranging from 1.5 to 2.2 m, with space between rows of 3.35 m and vine spacing of approximately

1.5 m along an east–west row orientation. In the interrow, the understory during the field measurements consisted of senescent grass stubble. Therefore, we assume minimal understory contributions to the canopy-scale carbon flux measurements during the observation period. This was also recently validated by Zahn et al. (2022) whose study of flux partitioning methods using eddy covariance tower measurements included RIP720 measurements.

Eddy covariance

Micrometeorological and carbon flux measurements were collected for the full growing season from each subplot using eddy covariance flux towers. Each of the four subplots were equipped with identical instrumentation located in the southeast corner of each subplot. The system was equipped with an integrated open path infrared gas analyzer and sonic anemometer, IRGASON (Campbell Scientific Inc., Logan, USA[1]) mounted 4.5 m above local ground level facing west. Fluxes were collected at 20 Hz and surface fluxes were estimated over 30 min time periods. Anomalous records in the high-frequency data were removed using a de-spiking moving window algorithm. Flux estimates were corrected by applying a two-dimensional coordinate rotation of the three wind speed components as well as for sensor displacement and frequency response attenuation. Sonic temperatures were corrected based on Schotanus et al. (1983), and the resulting fluxes were adjusted by the Webb, Pearman and Leuning (WPL) density corrections (Webb et al. 1980). Additional meteorological instruments were: an NR01 net radiometer (Hukseflux); an EE08 temperature and relative humidity probe (E + E Elektronik) in an aspirated shield (Apogee Instruments, Logan, USA); and soil moisture and temperature sensor (Stevens HydraProbe, Oregon, USA) installed at 5 cm depth (only soil temperature used).

Soil moisture

Near the center of each subplot, two CS655 soil moisture sensors (Campbell Scientific Inc., Logan, USA) were installed at a 30 cm depth. The soil moisture sensors were located about 30 cm apart from each other at either side of the vine row. Data were logged every 15 min. We averaged the two soil moisture readings together for subplot soil volumetric water content (VWC).

Air quality

Daily mean particulate matter (PM2.5 and PM10) data were downloaded from the US Environmental Protection Agency (EPA) Air Quality System Data Mart. The nearest monitoring station was located in Madera, CA (AQS Site ID: 06-039-2010; 36.953256° N, −120.034203° W), about 16 km northeast of the vineyards.

Tower-based spectrometer system

A single tower-based spectrometer system was located in the center of the four vineyard subplots. The spectrometer system was modified from the PhotoSpec system described in Grossmann et al. (2018) consisting of a 2D scanning telescope unit mounted at a height of 10 m for repeat targeted views. This telescope enables a narrow field of view (FOV) of 0.7°. However, for the entire duration of the experiment, an opal diffuser was used for all measurements to approximate a bi-hemispherical FOV to acquire average illuminated canopy spectra. Canopy spectra were determined using a Flame VIS–NIR Spectrometer (Ocean Optics, Inc., Orlando, FL, USA) with a 350–1000 nm wavelength range and 1.33 nm full width half maximum optical resolution.

Nine target locations were randomly selected for each vineyard plot covering sensor viewing angles of 30, 35, and 40° below horizon. For timely coverage, the camera rotated between subplots RIP1 through RIP4 (in order of RIP3, RIP1, RIP2, RIP4 and in reverse) every three targets, with a sky measurement (upward facing) between every six targets. At each target and sky measurement, multiple measurements occurred over a period of 60 s with integration time being auto adjusted to optimize signal to noise ratio and prevent saturation (at 80% signal saturation). A full cycle across all subplots (nine targets per plot; $n = 36$) took about 1.5 h and a semi-plot cycle (three targets per plot for single viewing angle, $n = 12$) took about 30 min.

Reflectance was calculated for each target measurement by dividing raw values by the corresponding sky measurement. From the spectral data, the normalized difference vegetation index (NDVI) and photochemical reflectance index (PRI) were calculated. NDVI was calculated as $\text{NDVI} = (R_{\text{NIR}} - R_{\text{Red}})/(R_{\text{NIR}} + R_{\text{Red}})$, where R_{NIR} is the average reflectance from 830 to 860 nm and R_{Red} is the average reflectance from 620 to 670 nm. PRI was calculated as $\text{PRI} = (R_{531} - R_{570})/(R_{531} + R_{570})$ where R_{531} is the average reflectance from 526 to 536 nm and R_{570} is the average reflectance from 565 to 575 nm.

We calculated half-hourly NDVI and PRI by averaging all targets per plot to the nearest half-hourly window to match the half-hourly eddy covariance measurements. Daily mean NDVI and PRI were determined from a solar-noon window between 11 and 16 h to minimize

Fig. 1 Phase angle effects of sun-sensor angles across all targets measurements between 11 and 16 h from July 21 to July 25 for NDVI (**a**) and PRI (**b**)
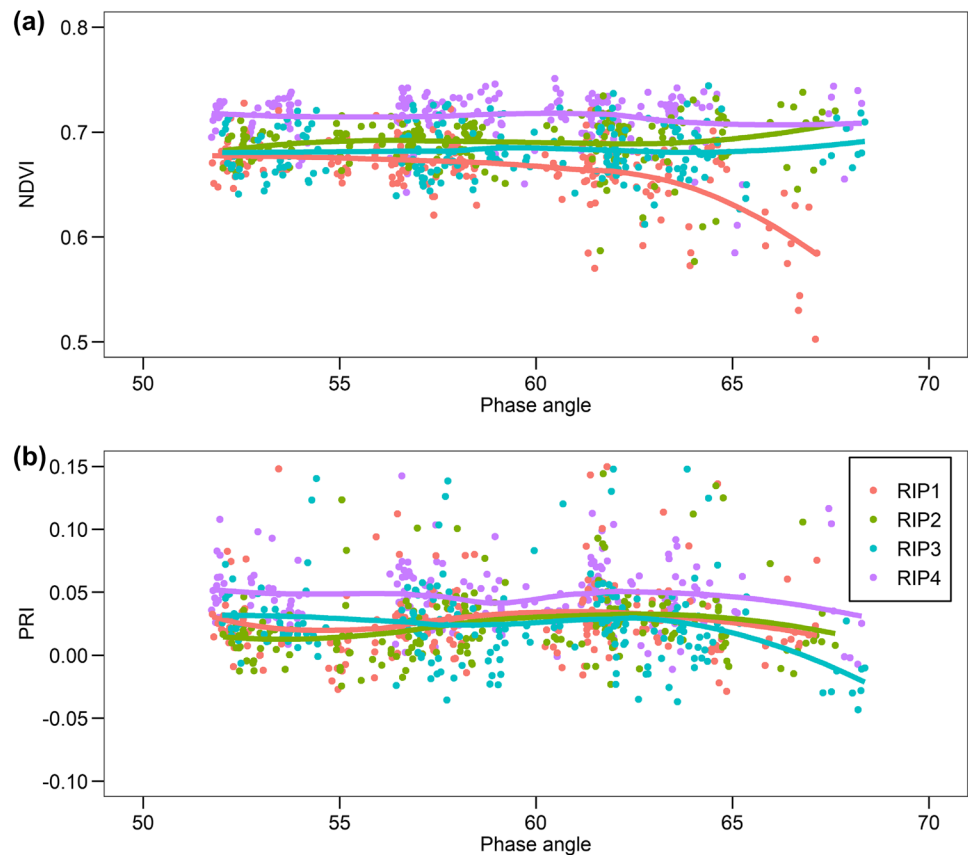
the influence of sun-sensor angular effects. To ensure that minimal sun-sensor angular effects, we calculated phase angle, which accounts for the angle between the sun and sensor (Doughty et al. 2019; Joiner et al. 2020). Phase angle incorporates the relative azimuth angle (RAA) between sensor viewing azimuth angle (VAA) and solar azimuth angle (SAA) relative to north in a clockwise direction (RAA = VAA − SAA). In addition, phase angle also accounts for solar zenith angle (SZA) and viewing zenith angle (VZA) and calculated as: Phase angle = $\cos^{-1}[\cos(SZA) \times \cos(VZA) + \sin(SZA) \times \sin(VZA) \times \cos(RAA)]$. Figure 1 shows minimal variation of NDVI and PRI across phase angles indicating a suitable window for daily means.

Stem water potential

From July 26 to August 2, 2020, stem water potential was measured between 11 and 16 h in 14–24 leaves per subplot. Fully matured leaves were placed in a reflective bag about 40 min prior to excision to prevent transpiration and allow the leaf to equilibrate with the stem. Water potentials were measured using a PMS Model 1505D pressure chamber (PMS Instrument Company, Albany, OR, USA).

Statistical analysis

In this study, we calculated daily means of solar noon from 11 to 16 h of the half-hourly eddy covariance data (GPP, air temperature, soil temperature, and vapor pressure deficit [VPD]), soil moisture (VWC) and the spectrometer system (NDVI and PRI). To smooth the data, we used 5-day running means. Based on the GPP timeseries, we identified four stress events characterized by a decline and recovery of daily GPP. The dates were selected using a stable baseline GPP chosen prior to a decline (stress response) and after a return to baseline (recovery) of the subplot averages. These events include an intensive observation period (IOP) from July 21 to Aug 6 where the four vineyard subplots underwent different watering regimes to induce drought stress (July 26 to Aug 2; see other papers in this issue). The remaining stress events were natural occurrences driven by environmental conditions including a heatwave (increased temperatures) and smoke (reduced incoming radiation caused by smoke from nearby wildfires): Stress Event 2 (Aug 6 to Aug 21; mostly heatwave); Stress Event 3 (Aug 21 to Sept 1; smoke); and Stress Event 4 (Sept 1 to Sept 14; temperature and smoke).

Statistical analyses were all performed in R (R Development Core Team 2020). To isolate the stress response and

recovery of GPP and PRI during each stress event and to minimize the influence of seasonal variation, we disentangled the short-term vs long-term responses by detrending the daily GPP, NDVI, and PRI values for each stress event using the pracma package (Borchers 2019). Detrending involves identifying a linear trend between two timepoints (identified using GPP and dates listed above) and subtract mean values from each data point to remove the linear trend. Random Forest analysis was used to identify variable importance for explaining the variation of GPP during the stress events. Variables included eddy covariance meteorological data, and air quality data (particulate matter [PM] 2.5 and 10) data. We used the Boruta package for Random Forest analysis (Kursa and Rudnicki 2010) to run iterations until all parameters were stabilized with a maximum iteration limit of 2000 times to determine variable importance via the mean decrease accuracy measure.

Results

During the growing season from July 19 to Sept 23, 2020, we identified the occurrence of four stress events based on a decline and recovery of GPP across all four grapevine subplots (Fig. 2a). These stress events were driven in part by a combination of environmental conditions that included air temperature, incoming global solar radiation, and soil moisture (Fig. 2). Enhanced temperatures were consistent across all stress events (Fig. 2b). During the IOP, the drip irrigation schedule was reduced to induce drought stress (Fig. 2d). Here, we observed declined levels of GPP, as well as decreased stem water potentials (Fig. 2f). Later in the season, Stress Events 2, 3, and 4, included variation of incoming global solar radiation that was mainly attributed to smoke from nearby fires that resulted in enhanced levels of PM10 and PM2.5 concentrations (Fig. 2e).

To further explore the contributions of environmental drivers to GPP variation, we utilized Random Forest analysis to evaluate relative variable importance (Fig. 3). For the Full Observation Period, all environmental conditions were important drivers in explaining GPP with VWC being the most important (Fig. 3a). For each of the stress events, the main environmental drivers varied as well as the explained variance percentage. For each stress event, the main environmental drivers for (Fig. 3b–e): IOP included air temperature, incoming radiation, VPD, and PM2.5; Stress Event 2 included air quality (PM2.5, PM10, and incoming radiation); Stress Event 3 included VWC and VPD; and Stress Event 4 included irrigation and VWC. The IOP and Stress Event 2 were best explained 83% and 63%, respectively, while Stress Events 3 and 4 were poorly explained 16% and 22%, respectively.

Continuous measurements of canopy-scale NDVI exhibited relatively consistent values across individual target measurements and stable values across all stress events during the growing season (Fig. 4a). In contrast, PRI varied between target measurements, and within and between stress events with all plots showing similar patterns (Fig. 4b). Within stress events, PRI generally showed a decline and recovery, similar to the patterns observed for GPP. However, during the entire observation period, PRI exhibited longer-term variation with general increases and declines across stress events. Due to the combination of both short- and long-term influences on the PRI signal, we detrended GPP, NDVI, and PRI for each stress event represented by the grey regions (Fig. 4). Detrending involves fitting a linear line to the data and removing the slope (Fig. 5a). This limits the variability of data to the short-term dynamics associated with the stress event and minimizes the influence of longer-term dynamics (Fig. 5b).

Detrending GPP, NDVI, and PRI per subplot for each predefined stress event highlights short-term stress response (Fig. 6). Stress events defined from GPP demonstrates the stress response (decline) and recovery (increase) representing near 40% of the total signal (Fig. 6a). In contrast, detrended NDVI showed an opposite pattern to detrended GPP, with an initial increase and subsequent decline, but the range of NDVI variation is very low (less than 3% of total signal) (Fig. 6b). Detrended PRI had a similar pattern to detrended GPP representing closer to 20–30% of the total signal (Fig. 6c). Between subplots, only detrended GPP during the IOP showed distinct differences between subplots, whereas detrended NDVI and PRI were unable to resolve differences between subplots with most values overlapping (Fig. 6). Interestingly, the detrended NDVI and PRI patterns during Stress Event 4 decoupled with the GPP pattern with multiple declines and recoveries (Fig. 6).

The relationships between GPP and PRI are shown in Fig. 7. Across the full observation period (Fig. 7a), the overall relationship between GPP and PRI was $R^2 = 0.25$ ($p < 0.001$). The relationships per subplot were slightly higher ($R^2 = 0.26$–0.37, $p < 0.001$). For each stress event (Fig. 7b–e), detrended GPP and PRI relationships were generally higher than across the full observation period with R^2 of 0.46, 0.47, and 0.33 for the IOP, Stress Event 2, and Stress Event 3, respectively. The individual relationships per subplot and response/recovery were generally much higher with an $R^2 > 0.50$ and ranging up to 0.92. The R^2 showed no bias towards response or recovery periods. Interestingly, Stress Event 4 had a non-significant overall relationship but at the response/recovery level, relationships of the stress response were high ($R^2 = 0.72$–0.89, $p < 0.05$), while recovery was non-significant (Fig. 7e).
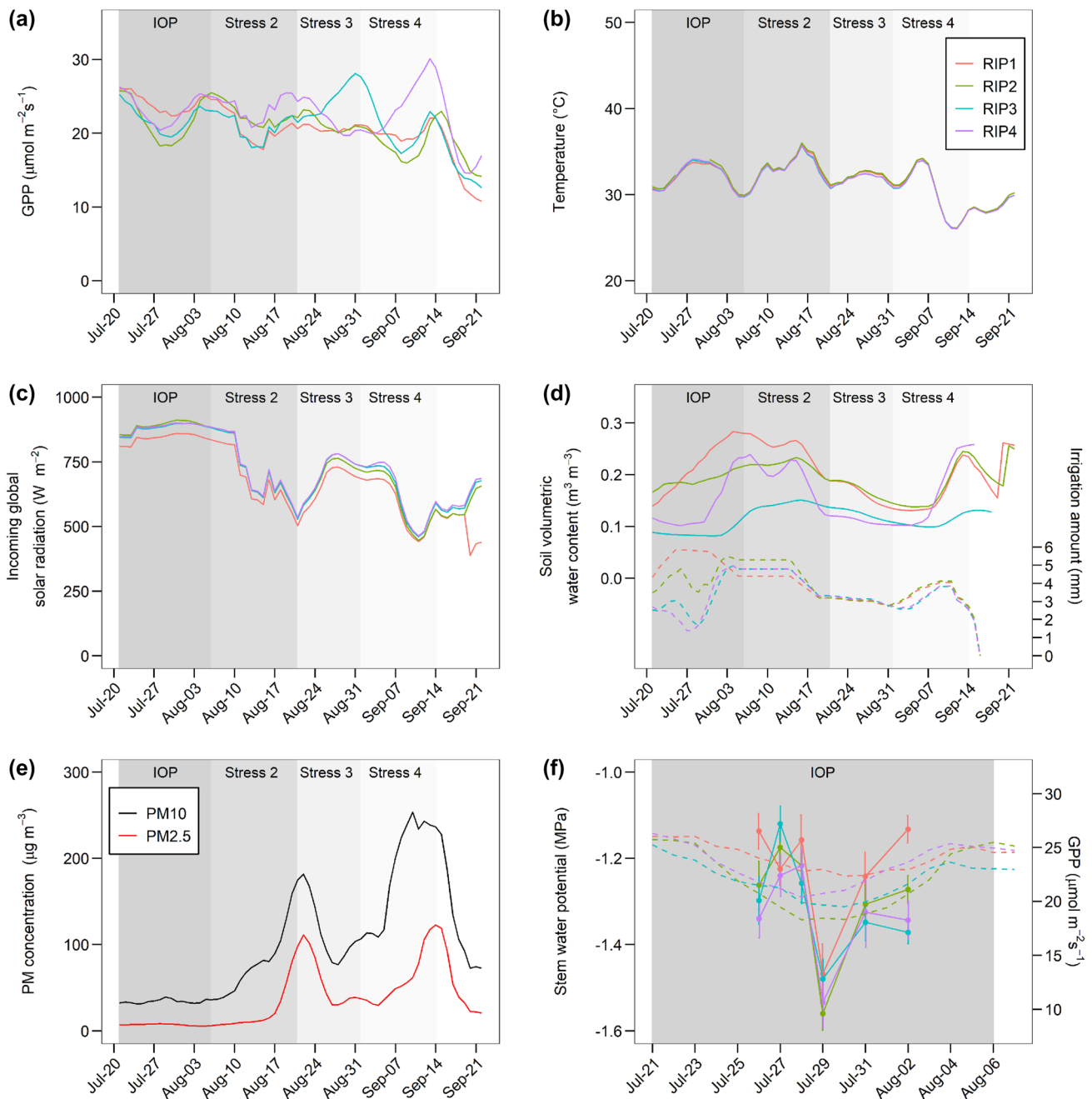
Fig. 2 Five-day running means of daily noontime gross primary productivity (GPP, **a**), air temperature (**b**), incoming radiation (**c**), 30 cm depth soil volumetric water content (solid line) and irrigation amount (dashed line) (**d**), particulate matter (PM) concentration (**e**), and dur-ing the intensive observation period (IOP) stem water potential (solid line) with GPP (dashed line) (**f**) for four vineyard subplots located in California's Central Valley. Stress events were defined based on GPP variation

Discussion

During the growing season, we observed four stress events based on the short-term response and recovery of GPP in all four vineyard subplots. These stress events were driven by changes in environmental conditions that included increased temperatures and low soil moisture (IOP) and decreased incoming radiation as a result of nearby wildfire (Stress Events 2, 3, 4), all of which can influence photosynthetic activity (Figs. 2, 3). The IOP was the only stress event unaffected by smoke, however, $PM2.5$ and $PM10$ were assigned relatively high predictor importance (Fig. 3b), which may be driven by a relatively minor increase that coincided strongly with GPP variation leading to enhanced importance
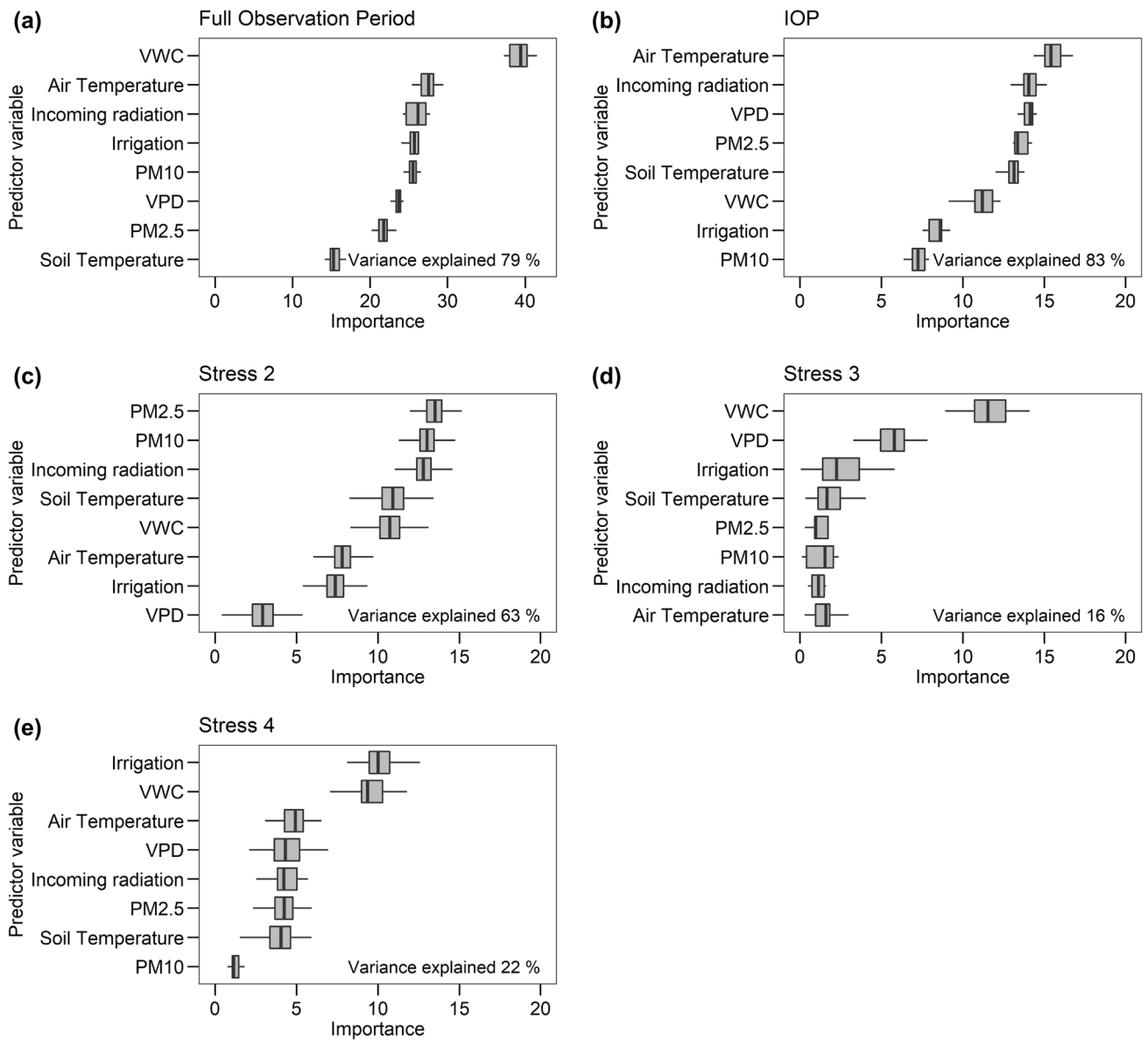
Fig. 3 Random forest analysis of relative variable importance for explaining variation of daily noontime gross primary productivity (GPP) for the Full Observation Period (**a**), Intensive Observation Period (IOP, **b**), Stress 2 (**c**), Stress 3 (**d**), and Stress 4 (**e**). Stress events were defined based on GPP variation. Abbreviations: *PM* particulate matter; *VPD* vapor pressure deficit; *VWC* volumetric water content

(Fig. 2e). In this study, we utilized tower-based optical-remote sensing to continuously monitor vineyard optical response during the stress events, we evaluated the potential of structural- (i.e. NDVI) and physiological-based (i.e. PRI) vegetation indices to reflect plant responses to environmental stress. Further, we applied detrending to disentangle short- and long-term variation of PRI to optimize detection of short-term stress events.

The structural- or greenness-based NDVI was unable to track the stress events (Fig. 4a), showing a slight (non-dynamic) decrease throughout the growing season. This is

likely due to small changes in canopy structure and biomass (e.g. loss of leaves, wilting), and greenness (chlorophyll degradation) over the course of the season, which are more severe symptoms from prolonged stress but also a common phenological trajectory observed in grapevines (Peñuelas et al. 1994; Haboudane et al. 2002; Zarco-Tejada et al. 2012). We did observe minor declines of NDVI between Stress Events 2 and 3 (Fig. 4b) that coincided with variations of incoming radiation and PM concentrations (Fig. 2c, e). This NDVI variation is potentially driven by smoke influence on radiation scatter or Rayleigh scattering, resulting

Fig. 4 Five-day running means of daily noontime normalized difference vegetation index (NDVI, **a**) and photochemical reflectance index (PRI, **b**) with gross primary productivity (GPP) for four vineyard subplots located in California's Central Valley. Solid thin lines represent target specific measurements of PRI and NDVI, solid thick lines represent plot specific means of PRI and NDVI, and dashed lines represent plot specific GPP. Stress events were defined based on GPP variation
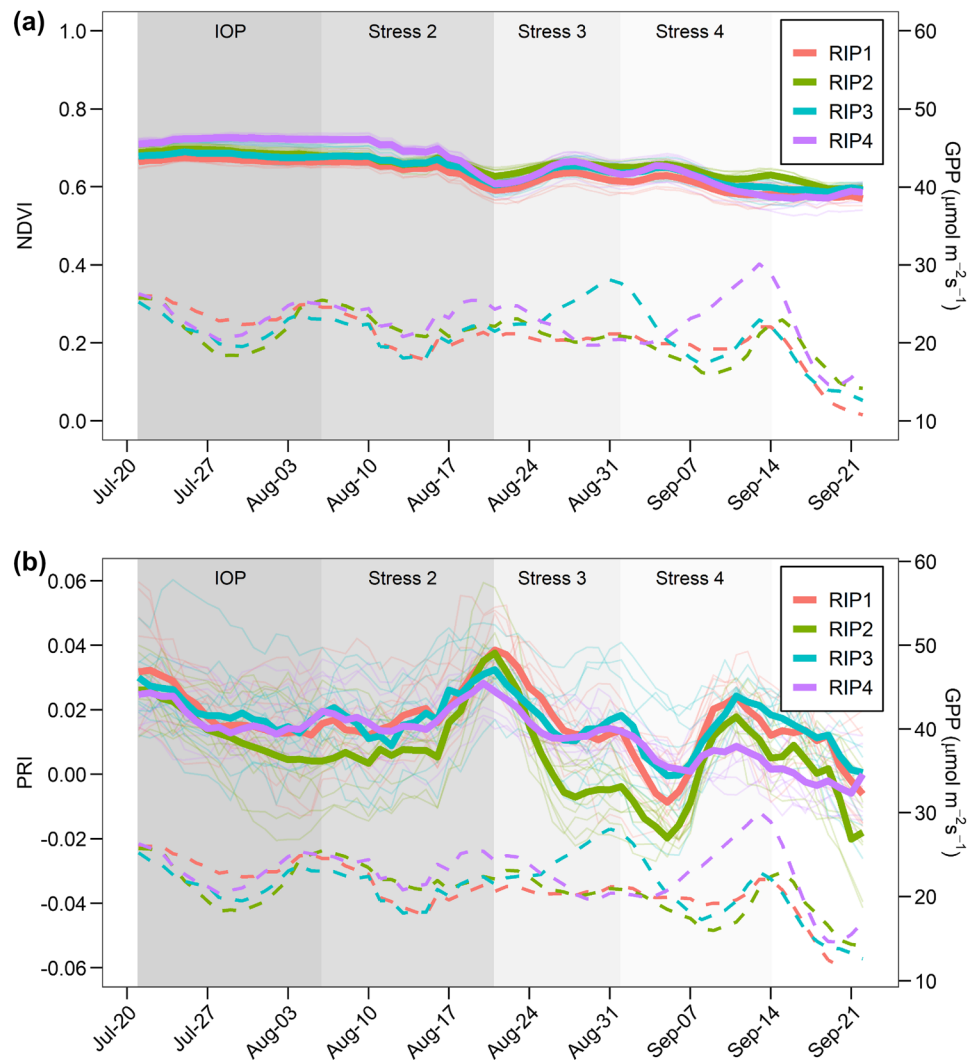
differential scattering of red wavelengths reflectance compared to near-infrared (NIR) wavelengths affecting NDVI calculation (Jones and Vaughan 2010). Detrending NDVI yielded minimal improvements for capturing stress events as it represented less than 3% of the total variation during stress (Fig. 6b). Therefore, NDVI is likely limited for detecting short-term stress events given the very subtle stress response (Fig. 4a) and sky condition constraints.

In contrast to canopy structure, early stress responses are generally linked to more physiological mechanisms such as stomatal closure which limits water loss and photosynthetic activity (Chaves et al. 2009). Given that the response of photosynthetic activity includes limitations by both stomatal closure and impairment to photosynthetic processes, ecosystem GPP itself may prove to be a robust indicator of stress across temporal scales (Flexas et al. 2004; Gambetta et al. 2020). Carotenoid pigments, specifically the xanthophyll cycle, are highly dynamic and involved in regulating photosynthetic activity and often used as an indicator

of light-use efficiency and non-photochemical quenching (Demmig-Adams and Adams 1996). PRI may exploit these physiological responses to perform as a proxy of photosynthetic activity and thus an indicator of short-term stress events. However, PRI is sensitive to both short-term changes in xanthophyll cycle and long-term changes in carotenoid/chlorophyll pigment pool (Garbulsky et al. 2011; Wong and Gamon 2015). Therefore, disentangling the short-term stress response and long-term seasonal response of PRI is needed to improve its performance (Hmimina et al. 2015). We utilized detrending to isolate the short-term PRI response contributed by the xanthophyll cycle (Fig. 5) and highlight a parallel response between detrended GPP and detrended PRI (Fig. 6).

The detrended GPP and PRI relationships differed between the four stress events (Fig. 7). The differences in the relationships and coefficient of determination (R^2) indicate a coupled stress response between GPP and PRI but there may be limitations in determining subplot differences in
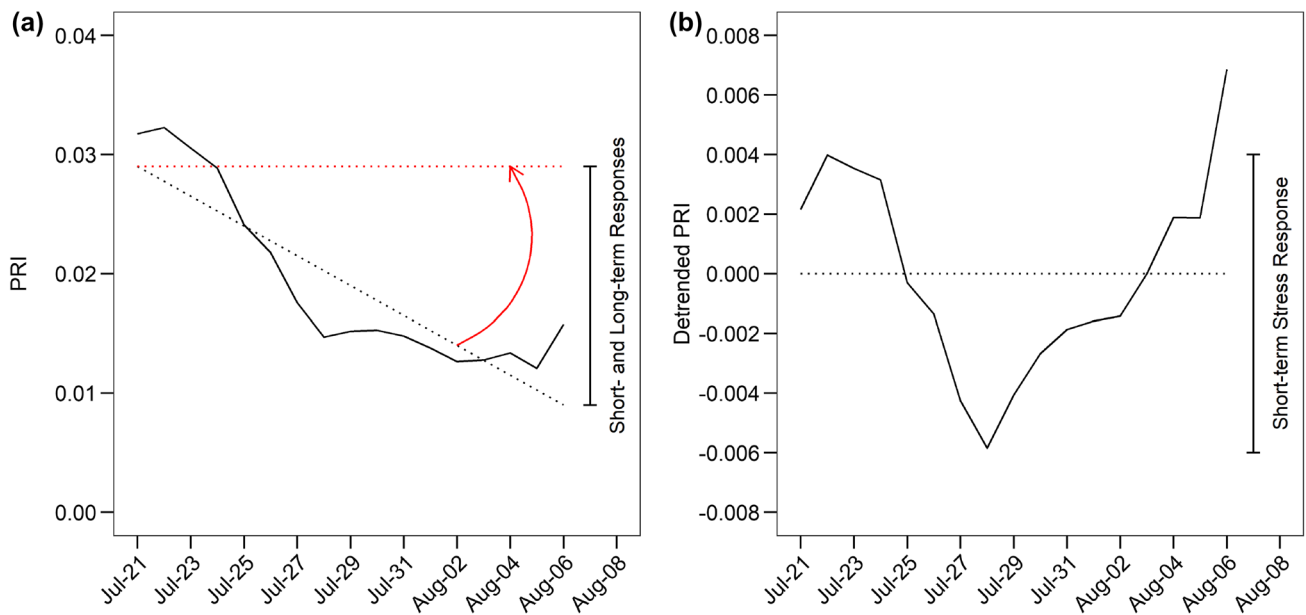
Fig. 5 Example of data detrending with the photochemical reflectance index (PRI) from RIP1 during the Intensive Observation Period (IOP). Left panel (**a**) shows raw PRI influenced by both short- (e.g. stress and xanthophyll cycle) and long-term signals (growth and pigment pools). By fitting a linear line through the data (black dot-ted line), the data are detrended by removing the slope of this fitted line (red dotted line). Right panel (**b**) shows the results of detrending, which highlights the short-term stress response of PRI by reducing long-term PRI responses. Stress events for detrending were defined based on GPP variation

magnitude or severity of stress response with PRI. In addition, out of the four stress events, the strongest GPP and PRI relationships were observed during the IOP and Stress Event 2, which were driven largely by temperature (Figs. 3, 7). In contrast, Stress Event 4 exhibited a poor overall relationship. Environmental drivers predicting GPP variation was also poor during Stress Event 4 (Fig. 3e) potentially due to the cumulative variation from air temperature, incoming radiation, VWC, irrigation, PM2.5, and PM10 (Fig. 2). Given that smoke likely reduced light for photosynthesis and also influenced the optical signal (Miura et al. 1998), we speculate an increased signal noise that reduced the optical signal quality which influenced both PRI and the GPP–PRI relationships during periods where smoke was present. This likely led to the weaker R^2 between GPP and PRI during Stress Event 2 recovery and Stress Event 3 response compared to their respective responses and recoveries (Fig. 7c, d). The IOP was the only stress event completely unaffected by smoke and air quality conditions and showed generally high R^2 between GPP and PRI for the response and recovery ranging from 0.53 to 0.92, except for RIP3 recovery, which was 0.18 (Fig. 7b). Given the relatively similar R^2 between the IOP and Stress Events 2 and 3, and generally overlapping lines of best fit, we suspect that PRI may be effective at tracking the stress response and recovery of grapevine GPP with little to no hysteresis effect, but more data will be needed.

Our optical-based approach demonstrated the potential of detrended PRI as an indicator of vineyard stress response and recovery of GPP. For assessing the magnitude and severity of stress, PRI may be limited and requires further evaluation as it was unable to reflect subplot specific magnitudes that GPP demonstrated during the IOP (Fig. 6), which was designed to apply an irrigation regime to the four subplots to induce different stress severity (Fig. 2). Further work may also include evaluating PRI as a proxy of light-use efficiency (Garbulsky et al. 2011) and to evaluate the impacts of solar and viewing angle on PRI (Hilker et al. 2008). Quantifying light-use efficiency and accounting for angular effects were beyond the scope of this paper as we utilized a diffuser to represent bi-hemispherical FOV for average canopy reflectance, limiting high precision measurements and viewing angle assessment. However, the large variation between targets (Fig. 4b), alludes to an angular influence impacting the magnitude of the PRI signal, but not temporal variation—even after limiting our data to solar noon (Fig. 1). In addition to optimizing PRI for stress quantification, there may be a complementary role for PRI with other remote sensing techniques such as thermal-based remote sensing for improved quantification of stress response and severity. Thermal-based products like the crop water stress index (CWSI) (Prueger et al. 2019) or evapotranspiration (ET) (Maes and Steppe 2012; Semmens et al. 2016; Knipper et al. 2019a; Anderson et al. 2021) track evaporative water loss. As thermal- and optical-based techniques are sensitive to different mechanistic processes (e.g. stomatal closure and photosynthetic activity, respectively), they offer potential complementation

Fig. 6 Detrended gross primary productivity (GPP, **a**), detrended normalized difference vegetation index (NDVI, **b**), and detrended photochemical reflectance index (PRI, **c**) for each stress event representing % variation of total signal. Detrending reduces the influence of seasonal variation by removing linear trends between two dates representing the timing of the stress events. Grey dashed lines show the partitioning of stress and recovery periods. The dates of the stress events and stress/recovery partitioning were determined based on the GPP data
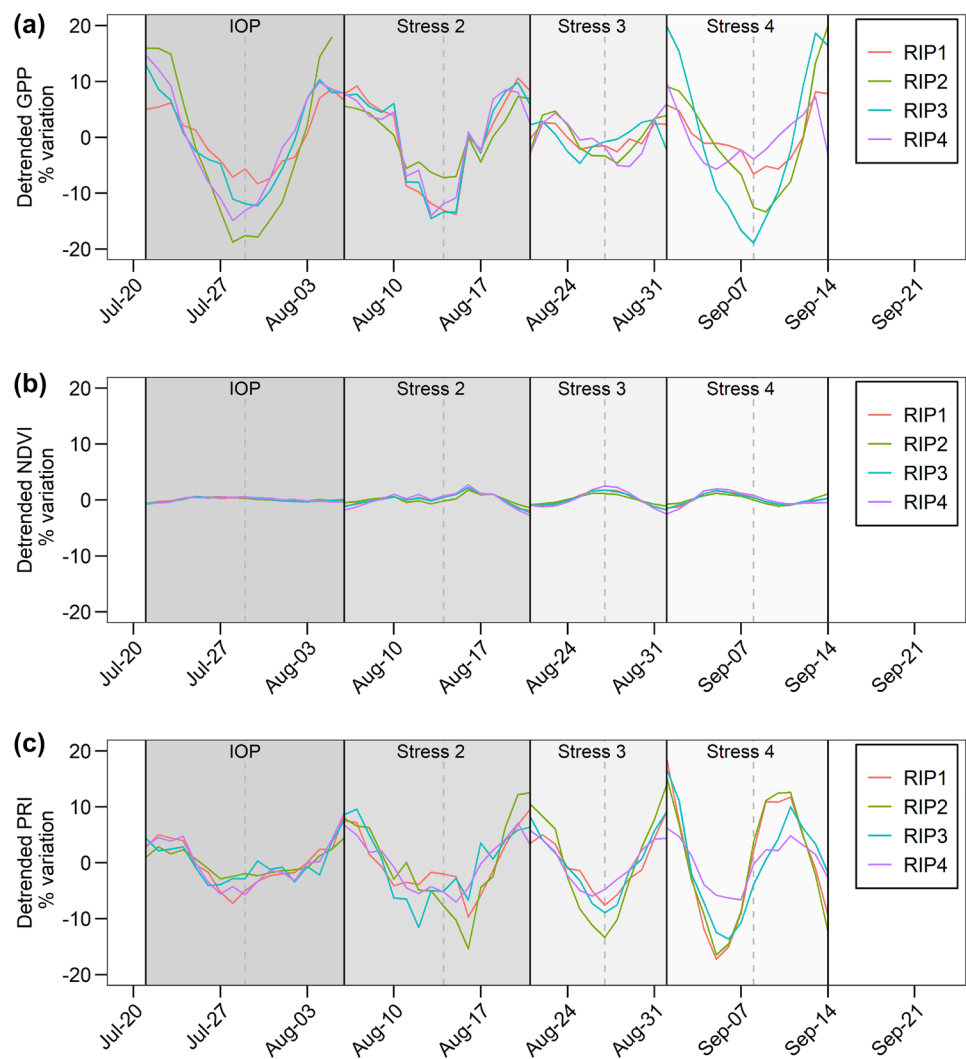
for detecting and quantifying the severity of stress events (Panigada et al. 2014). Another physiological remote sensing product, solar-induced fluorescence (SIF), represents physiological changes in absorbed light energy balance in relations to photosynthetic activity and excess energy dissipation (Porcar-Castell et al. 2014). SIF has shown promise for tracking drought events from satellite (Sun et al. 2015; He et al. 2019). Potentially, by utilizing PRI and/or SIF as a proxy of photosynthetic activity with thermal-based ET, a water-use efficiency (WUE) product may be developed based on remote sensing for continuous large spatial coverage of vegetation.

From a water management/irrigation scheduling perspective, having near real-time information on vine water use and stress is critical as well as providing a forecasting product to determine whether there is a likelihood for greater atmospheric demand the upcoming week. Irrigation is normally planned in weekly intervals, but for

stress detection, daily information is ideal and so fusion of multiple satellite sources is likely to be required to obtain near real-time information. In applying the thermal-based data fusion technique for irrigation scheduling, Knipper et al. (2019b) concluded that the method could detect the rapid decline in vineyard ET at both daily and weekly time steps; but the response was delayed, due to latencies in the availability of key Landsat 8 products. Alternatively, with optical-remote sensing, daily products of PRI in the form of the similar chlorophyll/carotenoid index (CCI) may be available from MODIS but is currently limited to large spatial areas of 1 km (Gamon et al. 2016), hence the use of tower-based instrumentation in this study. With tower-based instrumentation, low-cost PRI sensors may provide a cost-effective role as an indicator of stress events (Gamon et al. 2015). However, we note that post-processing steps, such as detrending, may be necessary to disentangle short- and long-term signals in the PRI for applied use.

Fig. 7 Relationships between daily noontime photochemical reflectance index (PRI) and gross primary productivity (GPP) across four vineyard subplots located in California's Central Valley for periods: Full observation period (**a**); Intensive observation period (IOP, **b**); Stress 2 (**c**); Stress 3 (**d**); Stress 4 (**e**). Black line for overall relationship across all subplots, solid line for stress and dashed line for recovery. Stress events were defined based on GPP variation. Significance codes: no asterisk $p > 0.05$; $*p < 0.05$; $**p < 0.01$; $***p < 0.001$
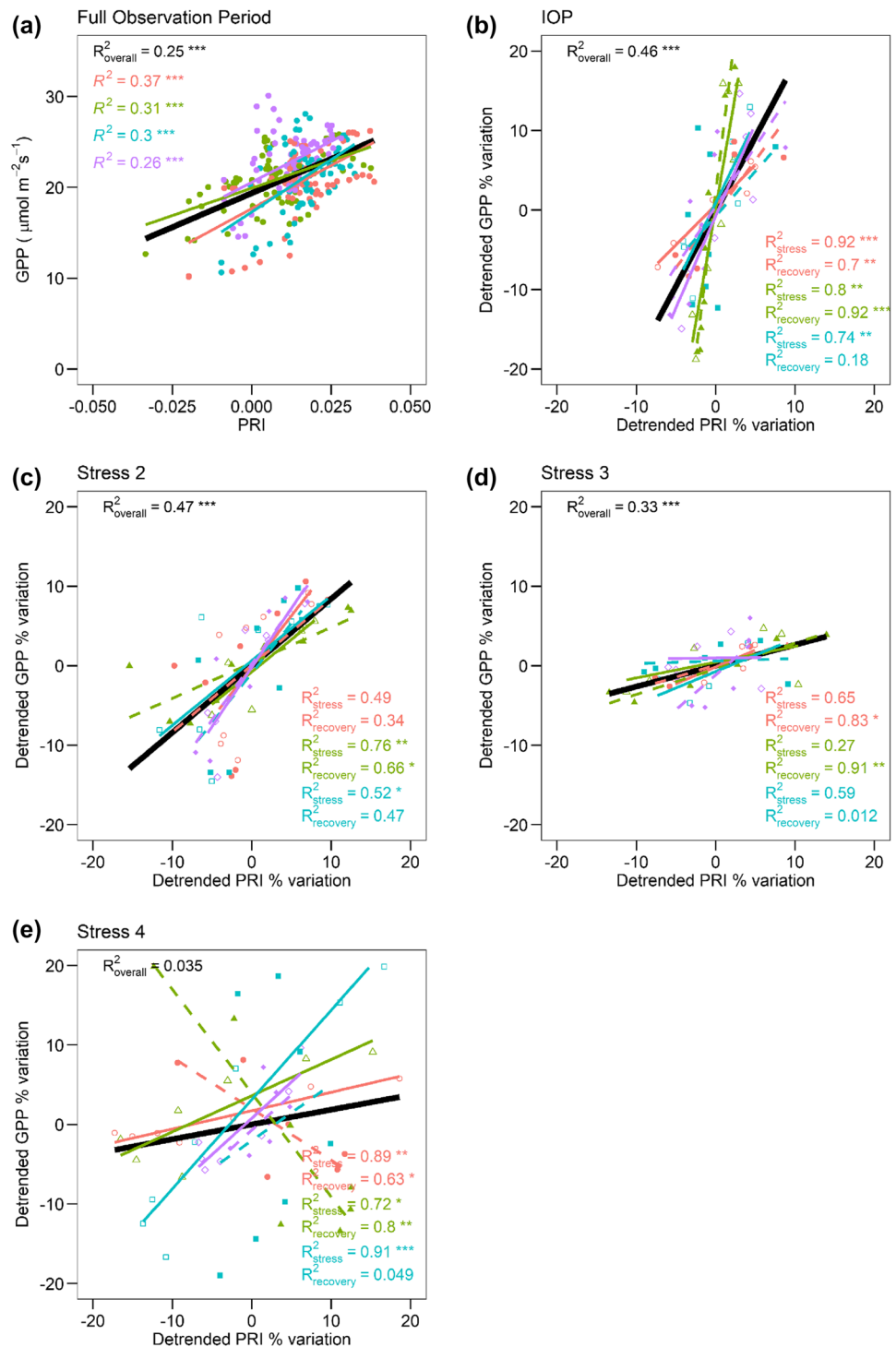
Conclusions

Our results offer an optical-remote sensing approach with PRI for monitoring vegetation stress response. Specifically for tracking short-term stress events, it is important to consider disentangling the PRI signal to optimize the detection of short-term PRI dynamics driven by the xanthophyll cycle and stress events. This will minimize confounding seasonal pigment pool effects on PRI since it is influenced by both short- (daily) and long-term (seasonal) adjustments in carotenoid pigment composition (Gamon and Berry 2012; Wong and Gamon 2015). Given the potential of optical-based remote sensing with high spatial and temporal coverage, tower-based systems provide a unique opportunity

to monitor sub daily information over seasonal periods, which should be further explored in detail for partitioning of short- and long-term vegetation dynamics. The ability to automate a monitoring system for both vegetation growth and stress response can benefit management and decision making, especially in regions with high irrigation management demands.

Declarations

Conflict of interest Authors report no conflicts of interest in the material presented in this study.

References

Alves I, Pereira LS (2000) Non-water-stressed baselines for irrigation scheduling with infrared thermometers: a new approach. Irrig Sci 19:101–106

Anderson MC, Yang Y, Xue J, Knipper KR, Yang Y, Gao F, Hain CR, Kustas WP, Cawse-Nicholson K, Hulley G et al (2021) Interoperability of ECOSTRESS and Landsat for mapping evapotranspiration time series at sub-field scales. Remote Sens Environ 252:112189

Bellvert J, Jofre-Ĉekalović C, Pelechá A, Mata M, Nieto H (2020) Feasibility of using the two-source energy balance model (TSEB) with sentinel-2 and sentinel-3 images to analyze the spatio-temporal variability of vine water status in a vineyard. Remote Sens 12:2299

Blackburn GA (2007) Hyperspectral remote sensing of plant pigments. J Exp Bot 58:855–867

Blum A (2017) Osmotic adjustment is a prime drought stress adaptive engine in support of plant production. Plant Cell Environ 40:4–10

Borchers HW (2019) pracma: practical numerical math functions

Buckley TN (2019) How do stomata respond to water status? New Phytol 224:21–36

Carlson TN, Ripley DA (1997) On the relation between NDVI, fractional vegetation cover, and leaf area index. Remote Sens Environ 62:241–252

Chaves MM, Flexas J, Pinheiro C (2009) Photosynthesis under drought and salt stress: regulation mechanisms from whole plant to cell. Ann Bot 103:551–560

Chaves MM, Zarrouk O, Francisco R, Costa JM, Santos T, Regalado AP, Rodrigues ML, Lopes CM (2010) Grapevine under deficit irrigation: hints from physiological and molecular data. Ann Bot 105:661–676

Demmig-Adams B, Adams WW (1996) The role of xanthophyll cycle carotenoids in the protection of photosynthesis. Trends Plant Sci 1:21–26

Doughty R, Köhler P, Frankenberg C, Magney TS, Xiao X, Qin Y, Wu X, Moore B (2019) TROPOMI reveals dry-season increase of solar-induced chlorophyll fluorescence in the Amazon forest. Proc Natl Acad Sci 116:22393–22398

Draper AJ, Jenkins MW, Kirby KW, Lund JR, Howitt RE (2003) Economic-engineering optimization for California water management. J Water Resour Plan Manage 129:155–164

Ficklin DL, Novick KA (2017) Historic and projected changes in vapor pressure deficit suggest a continental-scale drying of the United States atmosphere. J Geophys Res Atmos 122:2061–2079

Flexas J, Escalona JM, Medrano H (1998) Down-regulation of photosynthesis by drought under field conditions in grapevine leaves. Funct Plant Biol 25:893–900

Flexas J, Bota J, Cifre J, Escalona JM, Galmés J, Gulías J, Lefi E-K, Martínez-Cañellas SF, Moreno MT, Ribas-Carbó M et al (2004) Understanding down-regulation of photosynthesis under water stress: future prospects and searching for physiological tools for irrigation management. Ann Appl Biol 144:273–283

Gambetta GA, Herrera JC, Dayer S, Feng Q, Hochberg U, Castellarin SD (2020) The physiology of drought stress in grapevine: towards an integrative definition of drought tolerance. J Exp Bot 71:4658–4676

Gamon JA, Berry JA (2012) Facultative and constitutive pigment effects on the photochemical reflectance index (PRI) in sun and shade conifer needles. Israel J Plant Sci 60:85–95

Gamon JA, Peñuelas J, Field CB (1992) A narrow waveband spectral index that tracks diurnal changes in photosynthetic efficiency. Remote Sens Environ 41:35–44

Gamon JA, Serrano L, Surfus JS (1997) The photochemical reflectance index: an optical indicator of photosynthetic radiation use efficiency across species, functional types, and nutrient levels. Oecologia 112:492–501

Gamon J, Kovalchuck O, Wong C, Harris A, Garrity S (2015) Monitoring seasonal and diurnal changes in photosynthetic pigments with automated PRI and NDVI sensors. Biogeosciences 12:4149–4159

Gamon JA, Huemmrich KF, Wong CYS, Ensminger I, Garrity S, Hollinger DY, Noormets A, Peñuelas J (2016) A remotely sensed pigment index reveals photosynthetic phenology in evergreen conifers. Proc Natl Acad Sci 113:13087–13092

Garbulsky MF, Peñuelas J, Gamon JA, Inoue Y, Filella I (2011) The photochemical reflectance index (PRI) and the remote sensing of leaf, canopy and ecosystem radiation use efficiencies: a review and meta-analysis. Remote Sens Environ 115:281–297

Garrity SR, Eitel JUH, Vierling LA (2011) Disentangling the relationships between plant pigments and the photochemical reflectance index reveals a new approach for remote estimation of carotenoid content. Remote Sens Environ 115:628–635

Girona J, Mata M, del Campo J, Arbonés A, Bartra E, Marsal J (2006) The use of midday leaf water potential for scheduling deficit irrigation in vineyards. Irrig Sci 24:115–127

Gitelson AA, Peng Y, Arkebauer TJ, Schepers J (2014) Relationships between gross primary production, green LAI, and canopy

chlorophyll content in maize: implications for remote sensing of primary production. Remote Sens Environ 144:65–72

González-Dugo MP, Moran MS, Mateos L, Bryant R (2006) Canopy temperature variability as an indicator of crop water stress severity. Irrig Sci 24:233

Grossmann K, Frankenberg C, Magney TS, Hurlock SC, Seibt U, Stutz J (2018) PhotoSpec: a new instrument to measure spatially distributed red and far-red solar-induced chlorophyll fluorescence. Remote Sens Environ 216:311–327

Gu Y, Hunt E, Wardlow B, Basara JB, Brown JF, Verdin JP (2008) Evaluation of MODIS NDVI and NDWI for vegetation drought monitoring using Oklahoma Mesonet soil moisture data. Geophys Res Lett 35

Haboudane D, Miller JR, Tremblay N, Zarco-Tejada PJ, Dextraze L (2002) Integrated narrow-band vegetation indices for prediction of crop chlorophyll content for application to precision agriculture. Remote Sens Environ 81:416–426

He M, Kimball JS, Yi Y, Running S, Guan K, Jensco K, Maxwell B, Maneta M (2019) Impacts of the 2017 flash drought in the US Northern plains informed by satellite-based evapotranspiration and solar-induced fluorescence. Environ Res Lett 14:074019

Hilker T, Coops NC, Hall FG, Black TA, Wulder MA, Nesic Z, Krishnan P (2008) Separating physiologically and directionally induced changes in PRI using BRDF models. Remote Sens Environ 112:2777–2788

Hmimina G, Merlier E, Dufrêne E, Soudani K (2015) Deconvolution of pigment and physiologically related photochemical reflectance index variability at the canopy scale over an entire growing season. Plant Cell Environ 38:1578–1590

Ihuoma SO, Madramootoo CA (2017) Recent advances in crop water stress detection. Comput Electron Agric 141:267–275

Jackson RD, Idso SB, Reginato RJ, Pinter PJ (1981) Canopy temperature as a crop water stress indicator. Water Resour Res 17:1133–1138

Jackson RD, Kustas WP, Choudhury BJ (1988) A reexamination of the crop water stress index. Irrig Sci 9:309–317

Jaleel CA, Manivannan P, Wahid A, Farooq M, Al-Juburi HJ, Somasundaram R, Panneerselvam R (2009) Drought stress in plants: a review on morphological characteristics and pigments composition. Int J Agric Biol 11:100–105

Ji L, Peters AJ (2003) Assessing vegetation response to drought in the northern Great Plains using vegetation and drought indices. Remote Sens Environ 87:85–98

Joiner J, Yoshida Y, Köehler P, Campbell P, Frankenberg C, van der Tol C, Yang P, Parazoo N, Guanter L, Sun Y (2020) Systematic orbital geometry-dependent variations in satellite solar-induced fluorescence (SIF) retrievals. Remote Sens 12:2346

Jones GV, Davis RE (2000) Climate influences on grapevine phenology, grape composition, and wine production and quality for Bordeaux, France. Am J Enol Vitic 51:249–261

Jones HG, Vaughan RA (2010) Remote sensing of vegetation: principles, techniques, and applications. Oxford University Press, New York

Kasahara M, Kagawa T, Oikawa K, Suetsugu N, Miyao M, Wada M (2002) Chloroplast avoidance movement reduces photodamage in plants. Nature 420:829–832

Khanal S, Fulton J, Shearer S (2017) An overview of current and potential applications of thermal remote sensing in precision agriculture. Comput Electron Agric 139:22–32

Knipper KR, Kustas WP, Anderson MC, Alfieri JG, Prueger JH, Hain CR, Gao F, Yang Y, McKee LG, Nieto H et al (2019a) Evapotranspiration estimates derived using thermal-based satellite remote sensing and data fusion for irrigation management in California vineyards. Irrig Sci 37:431–449

Knipper KR, Kustas WP, Anderson MC, Alsina MM, Hain CR, Alfieri JG, Prueger JH, Gao F, McKee LG, Sanchez LA (2019b) Using high-spatiotemporal thermal satellite ET retrievals for operational water use and stress monitoring in a California vineyard. Remote Sens 11:2124

Kursa MB, Rudnicki WR (2010) Feature selection with the Boruta package. J Stat Softw 36:1–13

Kustas WP, Anderson MC, Alfieri JG, Knipper K, Torres-Rua A, Parry CK, Nieto H, Agam N, White WA, Gao F et al (2018) The grape remote sensing atmospheric profile and evapotranspiration experiment. Bull Am Meteor Soc 99:1791–1812

Maes WH, Steppe K (2012) Estimating evapotranspiration and drought stress with ground-based thermal remote sensing in agriculture: a review. J Exp Bot 63:4671–4712

Magney TS, Vierling LA, Eitel JUH, Huggins DR, Garrity SR (2016) Response of high frequency photochemical reflectance index (PRI) measurements to environmental conditions in wheat. Remote Sens Environ 173:84–97

Matthews MA, Anderson MM (1989) Reproductive development in grape (Vitis vinifera L.): responses to seasonal water deficits. Am J Enol Vitic 40:52–60

Miura T, Huete AR, van Leeuwen WJD, Didan K (1998) Vegetation detection through smoke-filled AVIRIS images: an assessment using MODIS band passes. J Geophys Res Atmos 103:32001–32011

Myneni RB, Williams DL (1994) On the relationship between FAPAR and NDVI. Remote Sens Environ 49:200–211

Panigada C, Rossini M, Meroni M, Cilia C, Busetto L, Amaducci S, Boschetti M, Cogliati S, Picchi V, Pinto F et al (2014) Fluorescence, PRI and canopy temperature for water stress detection in cereal crops. Int J Appl Earth Obs Geoinf 30:167–178

Patakas A, Nortsakis B (1999) Mechanisms involved in diurnal changes of osmotic potential in grapevines under drought conditions. J Plant Physiol 154:767–774

Peñuelas J, Gamon JA, Fredeen AL, Merino J, Field CB (1994) Reflectance indices associated with physiological changes in nitrogen- and water-limited sunflower leaves. Remote Sens Environ 48:135–146

Peñuelas J, Filella I, Gamon JA (1995) Assessment of photosynthetic radiation-use efficiency with spectral reflectance. New Phytol 131:291–296

Peters AJ, Walter-Shea EA, Ji L, Vina A, Hayes M, Svoboda MD (2002) Drought monitoring with NDVI-based standardized vegetation index. Photogramm Eng Remote Sens 68:71–75

Porcar-Castell A, Tyystjärvi E, Atherton J, van der Tol C, Flexas J, Pfündel EE, Moreno J, Frankenberg C, Berry JA (2014) Linking chlorophyll a fluorescence to photosynthesis for remote sensing applications: mechanisms and challenges. J Exp Bot 65:4065–4095

Prueger JH, Parry CK, Kustas WP, Alfieri JG, Alsina MM, Nieto H, Wilson TG, Hipps LE, Anderson MC, Hatfield JL et al (2019) Crop water stress index of an irrigated vineyard in the central valley of California. Irrig Sci 37:297–313

R Development Core Team (2020) R: a language and environment for statistical computing. R Foundation for Statistical Computing, Austria

Reddy AR, Chaitanya KV, Vivekanandan M (2004) Drought-induced responses of photosynthesis and antioxidant metabolism in higher plants. J Plant Physiol 161:1189–1202

Reynolds AG, Naylor AP (1994) 'Pinot noir' and 'Riesling' grapevines respond to water stress duration and soil water-holding capacity. HortScience 29:1505–1510

Sarlikioti V, Driever SM, Marcelis LFM (2010) Photochemical reflectance index as a mean of monitoring early water stress. Ann Appl Biol 157:81–89

Schotanus P, Nieuwstadt FTM, De Bruin HAR (1983) Temperature measurement with a sonic anemometer and its application to heat and moisture fluxes. Bound-Layer Meteorol 26:81–93. https://link.springer.com/article/10.1007/BF00164332

Semmens KA, Anderson MC, Kustas WP, Gao F, Alfieri JG, McKee L, Prueger JH, Hain CR, Cammalleri C, Yang Y et al (2016) Monitoring daily evapotranspiration over two California vineyards using Landsat 8 in a multi-sensor data fusion approach. Remote Sens Environ 185:155–170

Strzepek K, Yohe G, Neumann J, Boehlert B (2010) Characterizing changes in drought risk for the United States from climate change. Environ Res Lett 5:044012

Suárez L, Zarco-Tejada PJ, Sepulcre-Cantó G, Pérez-Priego O, Miller JR, Jiménez-Muñoz JC, Sobrino J (2008) Assessing canopy PRI for water stress detection with diurnal airborne imagery. Remote Sens Environ 112:560–575

Sun Y, Fu R, Dickinson R, Joiner J, Frankenberg C, Gu L, Xia Y, Fernando N (2015) Drought onset mechanisms revealed by satellite solar-induced chlorophyll fluorescence: insights from two contrasting extreme events. J Geophys Res Biogeosci 120:2427–2440

Tanaka SK, Zhu T, Lund JR, Howitt RE, Jenkins MW, Pulido MA, Tauber M, Ritzema RS, Ferreira IC (2006) Climate warming and water management adaptation for California. Clim Change 76:361–387

Thenot F, Méthy M, Winkel T (2002) The photochemical reflectance index (PRI) as a water-stress index. Int J Remote Sens 23:5135–5139

Ustin SL, Roberts DA, Gamon JA, Asner GP, Green RO (2004) Using imaging spectroscopy to study ecosystem processes and properties. Bioscience 54:523–534

Webb EK, Pearman GI, Leuning R (1980) Correction of flux measurements for density effects due to heat and water vapour transfer. Q J R Meteorol Soc 106:85–100

Wong CYS, Gamon JA (2015) Three causes of variation in the photochemical reflectance index (PRI) in evergreen conifers. New Phytol 206:187–195

Zahn E, Bou-Zeid E, Good SP, Katul GG, Thomas CK, Ghannam K, Smith JA, Chamecki M, Dias NL, Fuentes JD, Alfieri JG, Kwon H, Caylor KK, Gao Z, Soderberg K, Bambach NE, Hipps LE, Prueger JH, Kustas WP (2022) Direct partitioning of eddy-covariance water and carbon dioxide fluxes into ground and plant components. Agric For Meteorol 315:108790. https://doi.org/10.1016/j.agrformet.2021.108790

Zarco-Tejada PJ, Berjón A, López-Lozano R, Miller JR, Martín P, Cachorro V, González MR, de Frutos A (2005) Assessing vineyard condition with hyperspectral indices: leaf and canopy reflectance simulation in a row-structured discontinuous canopy. Remote Sens Environ 99:271–287

Zarco-Tejada PJ, González-Dugo V, Berni JAJ (2012) Fluorescence, temperature and narrow-band indices acquired from a UAV platform for water stress detection using a micro-hyperspectral imager and a thermal camera. Remote Sens Environ 117:322–337

Zarco-Tejada PJ, González-Dugo V, Williams LE, Suárez L, Berni JAJ, Goldhamer D, Fereres E (2013) A PRI-based water stress index combining structural and chlorophyll effects: assessment using diurnal narrow-band airborne imagery and the CWSI thermal index. Remote Sens Environ 138:38–50